Journal of Fluorine Chemistry 134 (2012) 35–43

Contents lists available at ScienceDirect

Journal of Fluorine Chemistry

journal homepage: www.elsevier.com/locate/fluor

About MX_3 and MX_2 (M^{n+} = Mg^{2+}, Al^{3+}, Ti^{4+}, Fe^{3+}; X^{p-} = F^-, O^{2-}, OH^-) nanofluorides

A. Demourgues *, N. Penin, D. Dambournet, R. Clarenc, A. Tressaud, E. Durand

Institut de Chimie de la Matière Condensée de Bordeaux-CNRS, Université Bordeaux, 87, Avenue du Dr. A. Schweitzer, 33608 Pessac Cedex, France

ARTICLE INFO

Article history:
Received 13 January 2011
Received in revised form 31 January 2011
Accepted 1 February 2011
Available online 15 March 2011

Keywords:
Inorganic fluorides
Nanomaterials
Mixed anions
Microwave synthesis
Structures
Powder XRD

ABSTRACT

Several nanosized fluoro-compounds have been prepared by microwave-assisted solvothermal routes: Al^{3+}-, Fe^{3+}- and Ti^{4+}-based oxyfluorides with the hexagonal tungsten bronze (HTB) framework, Ti^{4+}-based fluorinated anatase, and rutile MgF_2. The structural features have been determined using XRD and TEM analyses. The presence of OH^- groups substituted for F^- ions has been demonstrated for all of these nanofluorides. In Al- and Mg-based nanofluorides, the OH rate can be reduced by F_2-direct fluorination. Furthermore, the higher the polarizing power of the cation, the higher the oxygen content. For cation with high formal charge, such as Ti^{4+} stabilized in a distorted octahedral site, the occurrence of O^{2-}/OH^-/F^- anions in its vicinity as well as vacancies have to be mentioned. Finally coupling the microwave-assisted solvothermal route with the F_2-direct fluorination allow preparing high surface area metal fluorides where the amount of oxygen is noticeable and contribute to create under-coordinated cationic species at the surface which can induce high Lewis acidity.

1. One decade of inorganic fluorine chemistry at ICMCB-CNRS

During this last decade, a large range of new inorganic fluorinated compounds (either bulk fluorides or surface-modified materials) have been prepared at ICMCB-CNRS using various fluorination routes, involving either gas/solid reactions (F_2-direct fluorination up to 600 °C, anhydrous-HF up to 1100 °C), low-temperature radio-frequency (rf) plasmas with varied fluorinated gases, or microwave-assisted fluoro-solvothermal routes [1,2]. The resulting compounds were obtained as single crystals, powders or nanocrystallized phases. The physical chemical properties have been correlated to compositional and structural features. For instance, electronic properties of different types of fluorinated carbons and graphite intercalation compounds of fluorine and fluorides could be explained considering the formation of various types of ionic–covalent chemical bonding [3–5]. Surface properties of varied materials (oxide powders and ceramics, silica, C-based compounds, metals, polymers) have been modified allowing to fit with expected improvements (electronic conductivity, hydrophobic/hydrophilic balance) [6–8]. Very high fluorination level has been obtained for fluorinated silica and alumino-silicates by direct F_2-gas treatments [9,10]. Structural phase transitions in perovskite-derived phases and piezo-conductive behaviour of d-transition metal fluorides have been investigated [11–14]. The optical absorption properties in the UV–vis range of new oxyfluorides and oxyfluorosulfides have been also elucidated [15–17]. The optical band gap and refractive indices of these latter compounds could be tuned as a function of the metal–anion chemical bonding. Metal–fluorine chemical bonds have been more particularly investigated in high oxidation states transition metal and rare-earth fluorides, mostly cerium [18,19]. Finally, the chemical reactivity, Lewis acid–base behaviour and redox phenomena of nanofluorides based on Al, Ti or Fe have been studied considering the influence of surface area, chemical composition and structural features [20–24]. The knowledge of the inorganic frameworks is decisive as far as the metal–fluorine chemical bonding is a key-parameter to enhance electronic, optical and reactivity properties. Numerous applications of these new compounds could be anticipated such as UV-absorbers for wood protection or plastics, hydrophobic–hydrophilic layers for offset printing process, F_2 chemical storage and generation, purification agents in nuclear industry, heterogeneous catalysts with strong Lewis acidity.

2. Introduction

The development of new inorganic synthesis routes is required to optimize crystallites size as well as to stabilize new structural forms with specific compositions for new applications. Moreover during the last decades, the interest for nanoparticles in the fields of electronics, optics and heterogeneous catalysis has been growing. It is also crucial to avoid competing reactions leading to the stabilization of metastable phases and to control the chemical composition which depend on the crystallites size or surface area as well as the crystal structure and chemical bonding

* Corresponding author. Tel.: +33 05 40 00 26 55; fax: +33 05 40 00 27 61.
E-mail address: demourg@icmcb-bordeaux.cnrs.fr (A. Demourgues).

0022-1139/$ – see front matter © 2011 Elsevier B.V. All rights reserved.
doi:10.1016/j.jfluchem.2011.02.006

related to physical–chemical properties of these materials. Numerous works have been devoted to the synthesis and characterization of nanofluorides by sol–gel routes [25–29] or microwave-assisted solvothermal synthesis [23,30–33], despite the difficulty to get easily such nanoparticles because of the strong electronegativity and reactivity of fluorine that yields strong ionic bonds. Then, the use of metal alkoxides in organic medium or various solvents and metal precursors into aqueous-HF allows preparing high surface area metal fluorides. The case of Al trifluorides, crystallizing with the hexagonal-tungsten bronze (HTB) and used as heterogeneous catalysts in chlorofluorocarbon-substitutes, halogen exchange and in various fluoro-organic reactions, has been largely explored few years ago, because of the occurrence of strong Lewis acidic sites stabilized in these compounds [27,28,31,34]. Another issue is the thermal stability of nanofluorides and the effect of gas fluorination. Most of these catalytic reactions occur indeed at relatively high temperature ($T > 300\ ^\circ C$) and it is thus important to control the chemical composition and structural features of these nanofluorides related to their reactivity versus the temperature and the fluorinated atmosphere. As far as Al-based fluorides obtained by microwave-assisted solvothermal routes are concerned, the synthesis conditions, i.e. the choice of precursors, solvent, HF concentration and reaction temperature strongly influence the formation of various networks with different chemical compositions. The key role of OH^- groups substituting for F^- ions in the stabilization of the nanostructure has been demonstrated by FTIR and MAS-NMR spectroscopies. HTB frameworks and oxide fluorides with a general MX_3 chemical formula can be also obtained with transition metal such as Ti^{4+} or Fe^{3+}, in which OH^- groups and O^{2-} ions are still partially substituted for F^- ions [24]. This paper deals with the synthesis conditions of MX_3 compositions exhibiting nanosized domains and the identification of the structural features. The stability of Al^{3+} hydroxyfluorides as nanoparticles under elemental fluorine for different reaction temperatures has been also investigated. Moreover, MX_2 compositions crystallizing with rutile or anatase forms have been also obtained as nanofluorides with high surface area in the case of Ti^{4+} (anatase) or Mg^{2+} (rutile) cations. As far as MgF_2 nanoparticles are concerned, it will be shown how the oxygen content depending on the surface area may change as a function of F_2-direct fluorination temperature.

3. Experimental

3.1. Microwave-assisted solvothermal route

Actually inorganic syntheses can be thermally activated by conventional or microwave-assisted heating. The main interest of microwave-induced preparation consists in direct reactions at low temperature between reactants. Moreover microwave heating is generally faster, simple and energy efficient. Since the process is not limited by the thermal conductivity of the vessel, an instantaneous localized superheating of inorganic precursors, solvents, bases or acids which exhibit a dipolar polarization and/or ionic conduction (the two fundamental mechanisms for transferring energy from microwaves to the substance(s) being heated) can occur. Therefore, it provides a new processing technique to synthesize various inorganic materials. Three main interests of microwave-assisted route compared to conventional one can be raised:

- a faster route to access to crystallized phases,
- an improvement in numerous cases of the phase purity, homogeneity of the chemical composition and finally of the homogeneity in crystallites size,
- a favourable route to metastable- or kinetically stabilized phases.

Because of the ability of molecules to align with the applied electric field due to microwave interactions, the viscosity and the polarity of the solvent, the inorganic precursors and aqueous-HF are key parameters. Concerning the precursors, Al^{3+} and Fe^{3+} nitrates, Ti^{4+} oxychloride or isopropoxide and finally Mg^{2+} acetate have been tested, in order to tune the surface area. Depending on their dielectric constants ($\varepsilon = \varepsilon' + i\varepsilon''$) and energy loss ($\tan\delta = \varepsilon''/\varepsilon'$), various polar solvents such as water or isopropanol have been selected in order to control the surface area. Aqueous HF (Fluoric Acid, Rectapur, 40% min.) is the fluorinating agent. The successive stages of the process can be summarized as followed, the first one corresponding to an activation step:

(i) heating up to the synthesis temperature (90 °C or 160 °C) within five minutes,
(ii) heating step at 90 °C or 160 °C for 30′ or 120′,
(iii) cooling down to room temperature.

The second part of the synthesis corresponds to the drying stage and has been realized under argon gas stream followed by primary vacuum. In the case of Mg^{2+} cations, several centrifugations have been carried out in order to eliminate solvents and counter-ions followed by drying. The synthesis conditions of several compounds described in this paper are summarized in Table 1.

Experiments were conducted in a microwave-accelerated reaction system MARS5 (CEM corporation) operating at 2.45 GHz with a power supply varying in the 300–1200 W range, using XP-1500 vessels. The multimode instrument was equipped

Table 1
Synthesis conditions, surface area and structural parameters of metal oxyfluorides obtained by microwave-assisted solvothermal route.

Composition (chemical analysis)	Metal precursor	Solvents	[HF]/[M] molar ratio	Temperature (°C) and duration (min)	Surface area (BET) (m^2/g)	Space group	Cell parameters (Å)
$HSA\text{-}AlF_{2.6}(OH)_{0.4}$	Nitrate	Water/isopropanol = 1 (volume ratio)	3	160 °C and 120′	82	Cmcm	$a = 6.9681(2)$ $b = 12.0360(3)$ $c = 7.1434(1)$
$LSA\text{-}AiF_{2.4}(OH)_{0.6}$	Nitrate	Water/isopropanol = 6 (volume ratio)	3	160 °C and 120′	3	Cmcm	$a = 6.9494(2)$ $b = 12.0352(6)$ $c = 7.1328(8)$
$FeF_{2.2}(OH)_{0.8}$	Nitrate	Water	2	90 °C and 30′	–	Cmcm	$a = 7.3855(2)$ $b = 12.8176(3)$ $c = 7.5249(1)$
$Ti_{0.75}O_{0.25}(OH)_{1.3}F_{1.2}$	Oxychloride	Water	1.7	90 °C and 30′	–	$P6_3mmc$	$a = 7.397(3)$ $c = 7.597(3)$
$Ti_{1-x}O_{2-4x}(OH,F)_{4x}$	Isopropoxide	Isopropanol	1.7	90 °C and 30′	260	$I4_1/amd$	$a = 3.7964(3)$ $c = 9.5105(9)$
$MgF_{1.94}OH_{0.06}$	Acetate	Isopropanol	2	90 °C and 30′ (10%F_2, $T = 200$ °C)	116	$P4_2/mnm$	$a = 4.6258(6)$ $c = 3.0469(4)$

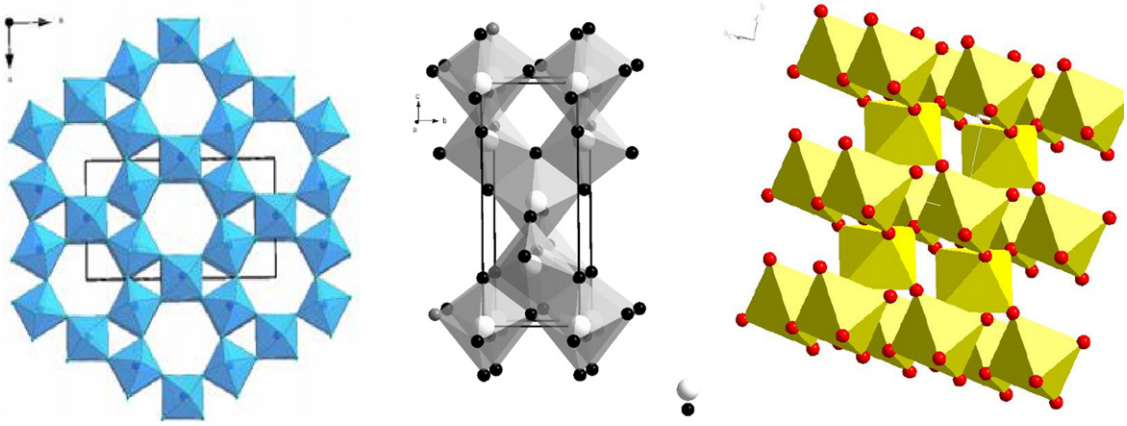

Fig. 1. Hexagonal tungsten bronze (HTB) MX_3 network, anatase and rutile MX_2 networks.

with temperature and pressure monitoring device (P_{max} = 55 bars, T_{max} = 220 °C).

3.2. F_2-gas fluorination treatment

Direct F_2-gas fluorination process was performed in dedicated fluorine equipment using special handling procedures previously described [35]. The sample was set in a passivated nickel boat. F_2-gas was diluted in argon (Air products). F_2 volume percentages in the fluorinating gas were set between 10 and 100% for reactions carried out between T = 200 °C and T = 500 °C.

3.3. Chemical analyses

The final [F]/[M] molar ratio was measured by electron probe micro-analysis (Castaing microprobe CECAMA SX 630 apparatus by Wavelength Dispersive Spectrometry) as well as by the CNRS Central Service of Analysis (F^- titration with specific electrode and M^{n+} by ICPMS). As far as the OH^- content substituting for F^- ions is concerned, the decomposition of the samples placed in graphite crucible at high temperatures, allows determining by FTIR spectroscopy the released CO rate directly related to the OH molar concentration.

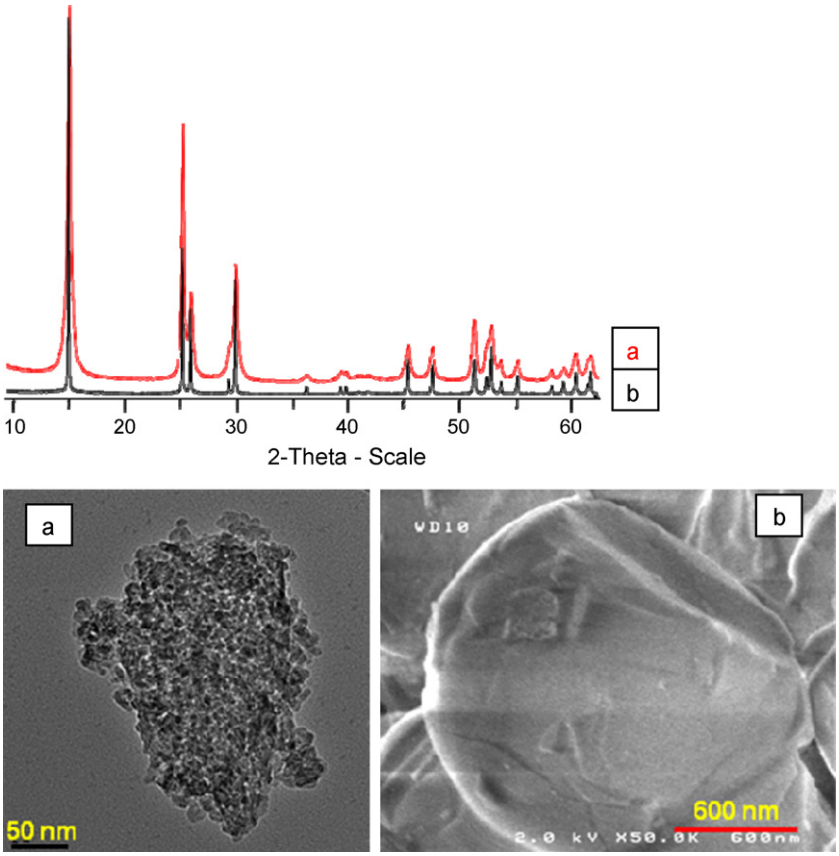

Fig. 2. X-ray diffractograms of HSA (a) and LSA (b) – HTB-$AlF_{3-x}(OH)_x$ compounds obtained by solvothermal routes. Scanning electron micrographs of HSA (a) and LSA (b) – HTB $AlF_{3-x}(OH)_x$ compounds.

3.4. X-ray diffraction analysis

Powder diffraction patterns were recorded on a PANalytical X'Pert Pro diffractometer in a Bragg–Brentano geometry (θ–2θ), using Ge(1 1 1) monochromated Cu-Kα_1 radiation (λ = 1.54051 Å). The investigated 2θ range was 10–110° with a step of 0.017° and a counting time of 1600 s per step. The whole pattern profile matching and Rietveld refinement were performed with the FULLPROF program. The X-ray line broadening analyses was performed by fitting the X-ray peak profile by using the pseudo-Voigt function of Thomson–Cox–Hastings and led to determine the average crystallite size and the degree of anisotropy.

3.5. Surface area determination

N_2 adsorption isotherms were performed at 77 K using an ASAP 2000 instrument from Micromeritics. The powder sample of mass around 200 mg was evacuated overnight at 573 K under 0.1 Pa prior to adsorption. The specific surface area S_{BET} was calculated from BET results applied in the P/P^o [0.03–0.25] range. Estimated standard deviations (e.s.d.) have been calculated for surface areas larger than 30 m^2/g and is equal to 5 m^2/g.

3.6. Scanning electron microscopy and transmission electron microscopy

Scanning electron microscopy (SEM) pictures were obtained with a FX 600 microscope. Surface charge elimination was achieved by silver deposition. Transmission electron microscopy (TEM) and electron diffraction experiments were performed with a JEOL 2000 FX microscope operating at 200 kV and using side-entry double tilt specimen stage. The maximum tilt angles available are ±45°. TEM samples were prepared by dissolving few milligrams of powder in ethanol. The solution was then dipped ten minutes into an ultrasonic bath so as to disagglomerate powder particles. One drop of the solution was finally deposited on a Formvar/Carbon copper grid.

3.7. ^{27}Al MAS-NMR spectroscopy

^{27}Al (I = 5/2) MAS NMR spectra were recorded using a 2.5 mm CP MAS probe at spinning speed 30–32 kHz on an Avance 750 Bruker spectrometer (B_0 = 17.6 T) operating at a ^{27}Al Larmor frequency of 195.5 MHz.

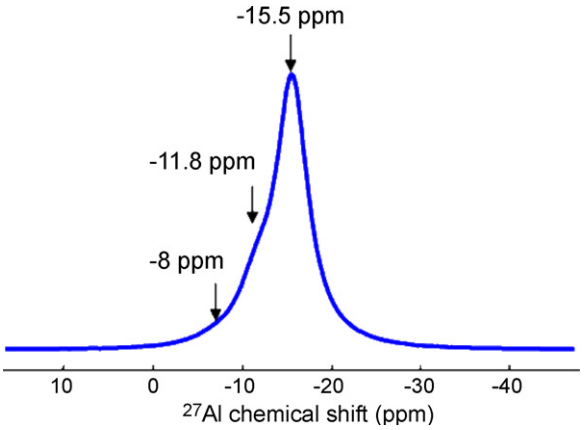

Fig. 3. ^{27}Al MAS-NMR spectrum of (HSA) HTB-$AlF_{3-x}(OH)_x$ compound. The chemical shifts of each contribution are noted.

3.8. Thermogravimetric analysis (TGA/MS)

The thermal degradation of the different compounds was followed by a thermogravimetric analyzer (TGA) (Setaram Setsys evolution) coupled with a mass spectrometer (MS) (Pfeiffer Ominstar) which allowed the detection of HF and water departure. Each sample was heated under helium atmosphere (heating rate 5 °C min^{-1}). The departure of water and hydroxyl groups starts before the fluorine species evolution.

4. Results

4.1. MX_3-HTB compounds

Al^{3+}, Ti^{4+} and Fe^{3+} compounds, crystallizing with hexagonal tungsten bronze (HTB) have been prepared by solvothermal routes (Fig. 1). The experimental parameters are collected in Table 1.

4.1.1. Al^{3+}-based fluorides

For Al^{3+} cation, isopropanol solvent was used at T = 160 °C where an exothermic reaction takes place. Such conditions allow tuning the crystallite size and the surface area around 100 m^2/g giving high surface area (HSA) Al-HTB fluoride. The following results have been detailed in a previous paper [23]. Comparison of

Table 2
Probability to have various $AlF_{6-x}(OH)_x$ species for different possible $AlF_{3-x}(OH)_x$ compositions. [The experimental contributions of each species (the chemical shifts of each contribution are noted as in Fig. 3) are determined by ^{27}Al MAS-NMR spectroscopy.].

Chemical composition	AlF_6	$AlF_5(OH)$	$AlF_4(OH)_2$	$AlF_3(OH)_3$	$AlF_2(OH)_4$
$AlF_{2.4}(OH)_{0.6}$	24%	41%	26%	8%	1%
$AlF_{2.5}(OH)_{0.5}$	32%	42%	21%	5%	---
$AlF_{2.6}(OH)_{0.4}$	41%	41%	15%	3%	---
	-15.5 ppm Exp. 83%		-11.5 ppm Exp. 14%	-8.0 ppm Exp. 3%	

Table 3
Variation of average crystallite size and degree of anisotropy in HSA $AlF_{3-x}(OH)_x$ versus F_2-gas fluorination temperature (see Fig. 4).

		T=300°C		T=400°C		T=500°C
Average size particle:	15 nm	→	16 nm	→	19 nm	→
Degree of anisotropy:	7 nm		8 nm		9 nm	

X-ray diffractograms and scanning electron micrographs show that crystallized compounds with microsized and nanosized domains can be thus synthesized (Fig. 2). The solvothermal route allows preparing HSA Al fluoride which corresponds to $AlF_{3-x}(OH)_x$ chemical composition where some OH groups have been substituted for fluorine. In the HTB network with an orthorhombic distortion (Cmcm space group), characterized by one-dimensional tunnels along the *c*-axis (Fig. 1), two non-equivalent Al atoms and four non-equivalent F atoms can be identified. In order to analyze the local environment of Al^{3+} cations, ^{27}Al MAS-NMR investigations have been performed. For the HSA-$AlF_{2.6}(OH)_{0.4}$ compound, in addition to the peak attributed to AlF_6 octahedra and corresponding to a chemical shift around −15 ppm, one can notice two shoulders at −12 and −8 ppm related to $AlF_{6-n}(OH)_n$ octahedra (Fig. 3). Considering the distribution of OH groups into two fluorine sites around the hexagonal tunnels where water molecules can be trapped, the probabilities to get $AlF_{6-n}(OH)_n$ octahedra can be determined on the basis of a binomial law (Table 2). Then, it is interesting to note the good agreement between the experimental data and this distribution leading to establish the occurrence of $AlF_{6-n}(OH)_n$ (*n*-integer = 0, 1, 2, 3) octahedral species and stabilized into the HTB network. From Table 2, it can be noted that the best agreement is obtained for $AlF_{2.6}(OH)_{0.4}$ composition. The XRD refinement of as-prepared HSA Al fluoride reveals the occurrence of platelets of 8 nm along the *a*-axis and 34 nm in the (*b*,*c*) plane, corresponding to an average crystallite size around 15 nm and a degree of anisotropy around 7 nm. One should have to notice that the thermal decomposition under N_2 or vacuum of $(NH_4)_3AlF_6$ or $AlF_3{\cdot}3H_2O$ fluorides leads to $AlF_{3-x}(OH)_x$ compounds with higher OH rate ($0.8 < x < 1$) [21] than those obtained by the microwave assisted solvothermal route, previously reported [23]. The thermal stability of Al hydroxyl-fluorides has been recently investigated. F_2-direct fluorination at $T = 300\,^{\circ}C$, 400 °C and 500 °C using pure elemental fluorine have been performed in order to conclude about the thermal stability and the variation of crystallite size and anisotropy. After thermal treatment under elemental fluorine, XRD patterns remain identical and both crystallite size and degree of anisotropy increase slightly versus temperature (Fig. 4 and Table 3). The remarkable stabilty of Al-fluoride with high surface area under pure elemental fluorine up to $T = 500\,^{\circ}C$ has to be outlined. Moreover, the ^{27}Al MAS-NMR study of HSA-$AlF_{2.6}(OH)_{0.4}$ annealed at 500 °C reveals the persistence of OH groups, corresponding to the $AlF_{2.8}(OH)_{0.2}$ composition. At $T > 600\,^{\circ}C$, the rhombohedral form of Al trifluoride (α-AlF_3, space group: R-3c) is obtained.

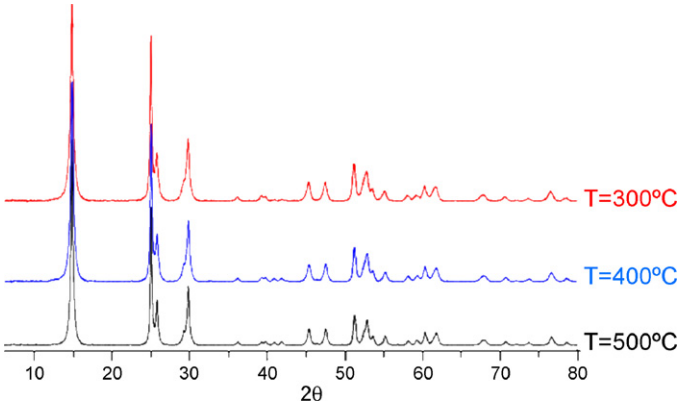

Fig. 4. X-ray diffractograms of (HSA) HTB-$AlF_{3-x}(OH)_x$ compound versus pure F_2-gas fluorination temperature.

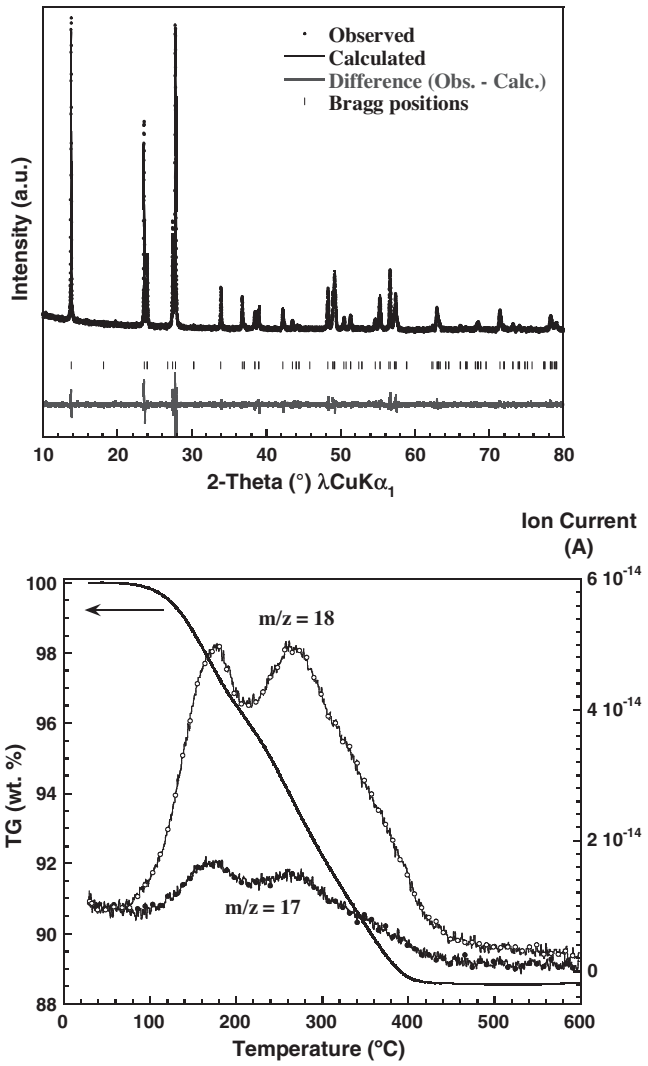

Fig. 5. XRD profile refinement of HTB $FeF_{3-x}(OH)_x(H_2O)_{0.33}$ compound obtained by solvothermal routes and MS-coupled TGA experiments of HTB $FeF_{3-x}(OH)_x(H_2O)_{0.33}$ showing the effects of OH groups.

4.1.2. Fe^{3+}-based fluorides

Well crystallized HTB-$FeF_{3-x}(OH)_x(H_2O)_{0.33}$ (Fig. 5) has been prepared by solvothermal process Starting from nitrates with an HF/M molar ratio equal to 2 in order to avoid the formation of $FeF_3{\cdot}3H_2O$ trifluoride trihydrate. In these conditions, shorter reactions occur at temperatures lower than in the case of HSA and LSA Al hydroxyfluorides. MS-coupled TGA measurements under He atmosphere reveal the occurrence of a large amount of OH groups stabilized in the HTB-network. At $T < 240\,^{\circ}C$, the weight loss (around 5%) is attributed to structural water ($0.33H_2O$) trapped in the hexagonal channel of the HTB framework. At $T > 240\,^{\circ}C$, the weight loss remains high, that is around 6.5%, and corresponds to the signature of OH groups ($m/z = 17, 18$) whereas the formation of hematite Fe_2O_3 is detected at $T > 350\,^{\circ}C$. It is important to point out that in these synthesis conditions, the OH amount in HTB-$FeF_{3-x}(OH)_x$ ($x \sim 0.8$ corresponding to a weight loss of $0.4H_2O$) is higher than in the HTB-$AlF_{3-x}(OH)_x$. Finally, TGA experiments tend also to show that the thermal stability is lower in the case of HTB-$FeF_{3-x}(OH)_x$. The sensitivity of hydrolysis and the polarizing character of Fe^{3+} ions should explain this behaviour. As for Al trifluoride, α-FeF_3 with rhombohedral symmetry is obtained for $T > 400\,^{\circ}C$.

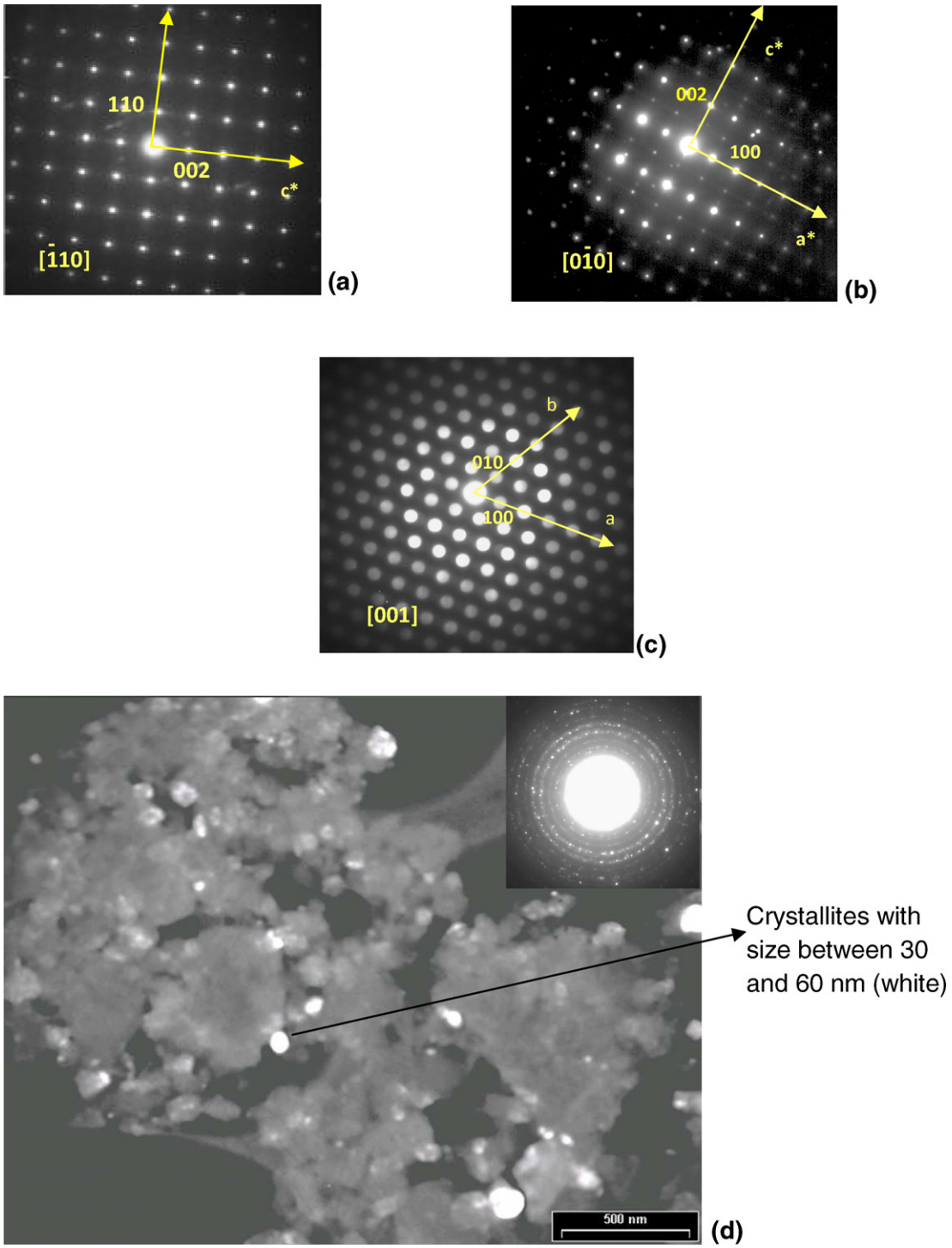

Fig. 6. TEM study of HTB-$Ti_{0.75}O_{0.25}(OH)_{1.3}F_{1.2}$ compound (a–c) and micrograph of crystallites (d) with size between 30 and 60 nm.

4.1.3. Ti^{4+}-based fluoride

Whereas Al^{3+} or Fe^{3+} HTB-trifluorides had been already described in the literature [36–39], a novel phase has been stabilized in the case of Ti^{4+}, starting from Ti oxychloride precursor with lowered HF/M molar ratio. In order to identify the crystal structure, electron diffraction experiments have been carried out. According to electron diffraction micrographs (Fig. 6), a six-fold axis is clearly identified and a hexagonal cell could be considered (a = 7.4 Å, c = 7.6 Å) from the observed reflection conditions: $h\,h\,l$: $l = 2n$ (0 0 l: $l = 2n$). The 0 0 1 spots appear are caused by a double diffraction phenomenon. The extinction conditions allowed us to conclude on the existence of a c glide plan and to propose only three possible space groups: $P6_3/mmc$, P-62c and $P6_3mc$. In addition one should notice that the powders are very well crystallized and crystallites sizes vary from 50 to 70 nm. The first 20 lines of the X-ray powder diffraction pattern, with an absolute error of 0.03° (2θ) on peak positions, were indexed on the basis of an hexagonal solution ($P6_3/mmc$ space group), with the unit-cell parameters a = 7.3968(6) Å; c = 7.5974(4) Å, which are related to the hexagonal tungsten bronze family. The real HTB network adopts the $P6_3/mcm$ space group for instance for M_xWO_3 (M = Cs, K and $x \sim 0.2$–0.3) with the c glide plane perpendicular to the (h 0 l)

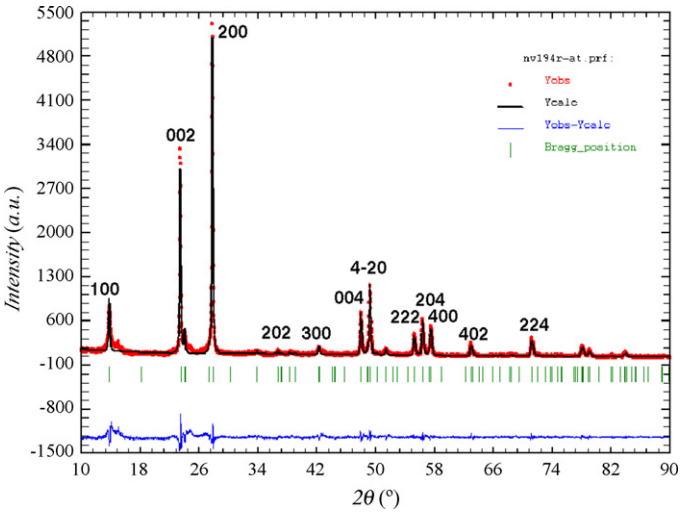

Fig. 7. XRD profile refinement of HTB $Ti_{0.75}O_{0.25}(OH)_{1.3}F_{1.2}$ compound.

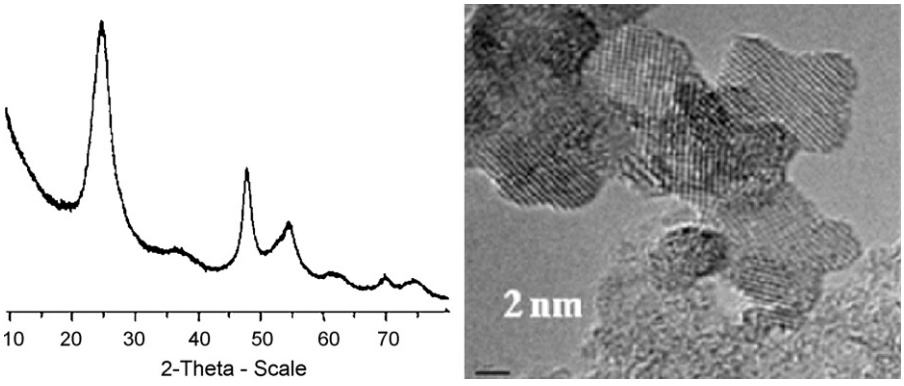

Fig. 8. X-ray diffractogram (a) and HRTEM image (b) of HSA Ti-based oxy-hydroxy-fluoride ($Ti_{1-x}O_{2-4x}(OH,F)_{4x}$) with anatase form.

direction. Thus, the difference must be associated to the tilting of octahedra where Ti^{4+} cations occupy the center of these octahedral sites. On the basis on this primitive hexagonal unit-cell, the profile of X-ray diffraction pattern could be refined considering the Laue class 6/mmm and the most symmetrical space group ($P6_3/mmc$) corresponding to the average chemical formula $TiO(OH,F)_2$. The results of this refinement and indexations are reported in Fig. 7. Actually, chemical analyses, density measurements and Rietveld refinement (neutron and X-ray diffractions) allow concluding about the occurrence of defects such as cationic and anionic vacancies leading to the following chemical formula $Ti_{0.75}O_{0.25}(OH)_{1.3}F_{1.2}$. Finally TGA measurements confirm the high OH amount with a weight loss larger than 10% at $T > 120\ ^\circ C$ and a fluorine departure at $T > 250\ ^\circ C$ showing that Ti oxy-hydroxy-fluoride is less stable than Fe^{3+} hydroxy-fluoride. The higher polarizing character and formal charge of Ti^{4+} which are at the origin of the poor stability of this compound, lead also to the stabilization of O^{2-} anions in Ti^{4+} vicinity.

4.2. MX_2 anatase and rutile compounds

As far as Ti^{4+} ions are concerned, the use of isopropoxide as precursor and isopropanol as solvent enables the preparation of fluorinated anatase form with high surface area (HSA = 260 m^2/g). The kinetics of fluorination and the formation of various frameworks are strongly influenced by the nature of precursors/solvents and ligands, while keeping the same HF/Ti molar ratio as for the synthesis of Ti-HTB oxy-hydroxy-fluoride. The XRD pattern can be indexed on the basis of the tetragonal cell related to the anatase form (Figs. 1 and 8 and Table 1). Taking into account the full width at half maximum (FWHM) of X-ray diffraction lines, one

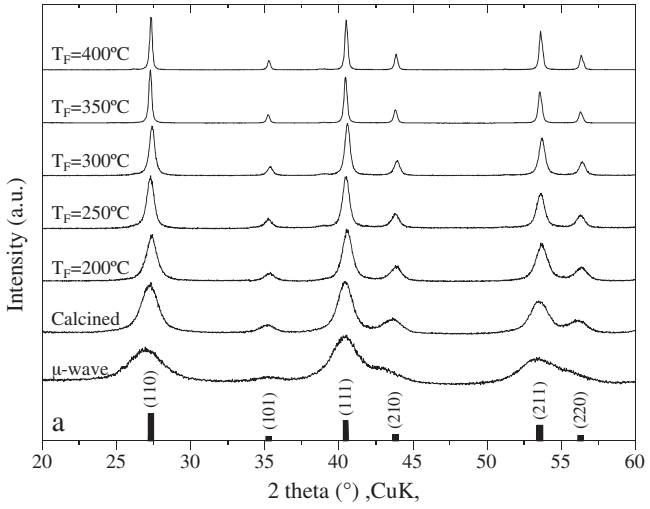

Fig. 9. X-ray diffraction powder patterns of MgF_2 after microwave-assisted solvothermal synthesis, calcination at 300 °C under argon and F_2-direct fluorination (10% F_2/90% Ar) at several temperatures.

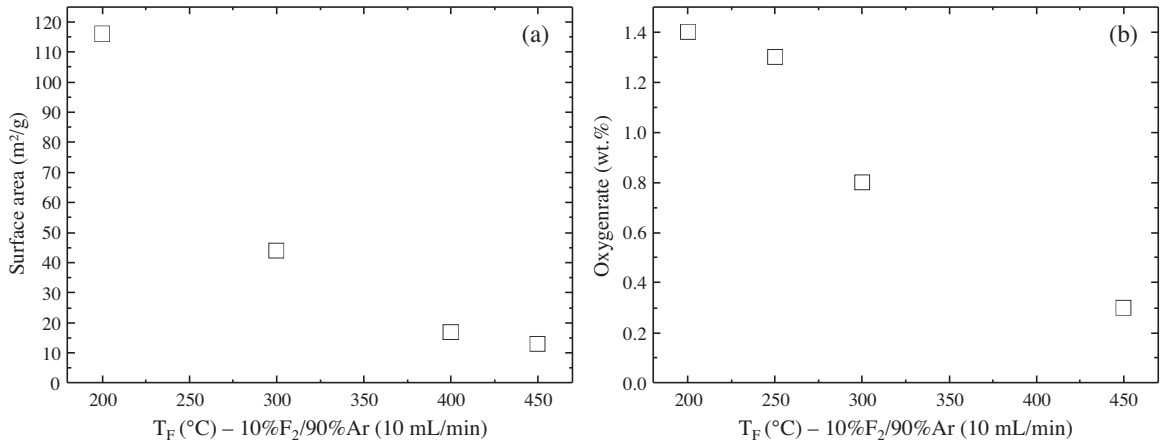

Fig. 10. Variations of the surface area (a) and the oxygen rate (b) versus the temperature of the F_2-direct fluorination step for $MgF_{2-x}(OH)_x$ compositions.

Table 4
Surface area (SA), oxygen rate, average crystallite size of $MgF_{2-x}(OH)_x$ compounds versus F_2-gas fluorination temperatures (see Fig. 10).

T_F (°C)	SA (m^2/g)	Oxygen rate (wt.%)	Crystallite size (nm)
200	116	1.4	9
250	–	1.3	13
300	44	0.8	19
400	17	–	38
450	13	0.3	49

should notice that the coherent domains are very small, in good agreement with the HRTEM observations showing crystallite dimensions around 5 nm and corresponding indeed to anatase symmetry. Finally chemical analyses show that the OH and F contents remain high in this compound, leading to consider the following chemical formula $Ti_{1-x}O_{2-4x}(OH,F)_{4x}$ with the occurrence of Ti vacancies as for Ti-HTB oxy-hydroxy-fluoride. In all as-prepared Ti compounds, the existence of Ti vacancies has to be pointed out. The high polarizing character of Ti^{4+} cations may be responsible of the stabilization of various kinds of anions (F^-, O^{2-}, OH^-) in their vicinity and to observe distorted environments. Furthermore, in anatase network with octahedra zig-zag chains, Ti edge-sharing octahedral sites (Fig. 1) undergo stronger distortion than corner-sharing octahedra in HTB framework.

The last example concerns MgF_2 as rutile-type structure (Fig. 1) which has been already investigated through sol–gel routes [29,40,41]. Prepared by microwave-assisted solvothermal route it exhibits high surface area, larger than 100 m^2/g. As for the previous compounds, the occurrence of hydroxyl groups in the vicinity of Mg^{2+} cations, revealed by chemical analysis, TGA measurements, FTIR analysis or ^{19}F and ^1H MAS-NMR studies, can be established. The effect of F_2-gas fluorination temperature (10% F_2/90% Ar) on MgF_2 crystallinity has been represented in Fig. 9. The higher the treatment temperature, the lower the FWHM of X-ray diffraction lines and the higher the coherent domain or the crystallite size. After F_2-direct fluorination at $T = 200$ °C, the chemical composition is $MgF_{1.94}(OH)_{0.06}$ with a much lower OH content compared to Al, Fe or Ti-based compounds, due to the more electropositive character of Mg^{2+} cations which prefer more electronegative anions such as F^-. Then, the surface area decreases with an asymptotic law as a function of the F_2-direct fluorination temperature (Fig. 10). Furthermore, the lower the surface area, the lower the oxygen content (Fig. 10 and Table 4) thanks to a higher F_2-treatment temperature. In rutile-type network with edge-sharing and corner-sharing octahedra, higher contents of OH groups for HSA-MgF_2, probably stabilized at the surface of nano-domains, contribute to create under-coordinated Mg^{2+} cations at the surface associated to anionic vacancies as revealed by FTIR analysis and TGA measurements. The stabilization of such anionic vacancies due to the OH departure can be found in HTB network with corner-sharing octahedra or in anatase form with only edge-sharing octahedral sites.

5. Conclusions

By coupling microwave-assisted solvothermal synthesis and F_2-direct fluorination, Al^{3+} and Mg^{2+} nanofluorides have been synthesized. The amount of OH^- groups substituted for F^- ions remains noticeable and higher in the case of Al^{3+} which is more electronegative and have a stronger affinity for oxygen than Mg^{2+} cations. Moreover, it has been demonstrated that HTB-network can accommodate a larger content of OH groups because of the occurrence of 1D-tunnels where water molecules can be trapped. In the case of Fe^{3+}, $FeF_{3-x}(OH)_x$ hydroxy-fluorides with the HTB framework contain a larger amount of hydroxyl groups than HTB Al hydroxy-fluoride because of the higher electronegativity and polarizing character of Fe^{3+} cations, as well as its stronger affinity for hydrolysis. In the case of the new Ti^{4+}-HTB network, hexagonal unit cell has been determined whereas orthorhombic unit cells have been found in the case of Al^{3+} and Fe^{3+}. Moreover, the Ti^{4+} HTB nanofluoride exhibits structural defects, with O^{2-} and OH^- substituting for F^- anions. The higher formal charge of Ti^{4+} should explain the stabilization of O^{2-} in its vicinity and it is impossible to avoid the occurrence of oxygen in such nanofluorides following the proposed synthesis route. Finally it is also the case for Ti-based nanofluorides with anastase form, in which highly divided (HSA = 260 m^2/g) materials can be obtained. In these edge-sharing octahedra forming zig-zag chains, the Ti^{4+} site are locally distorted with various anions (F^-, O^{2-}, OH^-) in its vicinity. The case of Ti vacancies have been already mentioned in the case of cubic ReO_3-type $Ti_{0.75}(OH)_{1.5}F_{1.5}$ hydroxyfluoride where the high polarizing power of Ti^{4+} is probably the key parameter at the origin of the creation of vacancies [2,24,42]. Moreover in both Ti^{4+}-based nanofluorides, the stabilization of cationic vacancies has to be considered in order to explain defects structure and to verify electroneutrality equation. Moreover the occurrence of oxygen stabilized in these nano-fluorides contribute to generate at the surface under-coordinated cationic species in the case of Al^{3+}, Fe^{3+}, Ti^{4+} and why not Mg^{2+} where the OH^- rate remains the lowest.

Acknowledgments

J. Magimel and F. Weill (ICMCB-CNRS) are acknowledged for SEM and HRTEM experiments, and C. Legein, from LOF, Université du Maine, France for solid-state NMR.

References

[1] T. Nakajima, B. Zemva, A. Tressaud (Eds.), Advanced Inorganic Fluorides, Elsevier, 2000.
[2] D. Dambournet, A. Demourgues, A. Tressaud, in: A. Tressaud (Ed.), Functionalized Inorganic Fluorides: Synthesis, Characterization and Properties of Nanostructured Solids, Wiley, 2010, pp. 39–68;
A. Demourgues, L. Sronek, N. Penin, Functionalized Inorganic Fluorides: Synthesis, Characterization and Properties of Nanostructured Solids, 2010, pp. 229–271.;
A. Demourgues, E. Lataste, E. Durand, A. Tressaud, Functionalized Inorganic Fluorides: Synthesis, Characterization and Properties of Nanostructured Solids, 2010, pp. 519–543.
[3] A. Tressaud, T. Shirasaki, G. Nansé, E. Papirer, Carbon 40 (2002) 217.
[4] T. Nakajima, V. Gupta, Y. Ohzawa, M. Koh, R.N. Singh, A. Tressaud, E. Durand, J. Power Sources 104 (2002) 108.
[5] A.V. Kepman, V.F. Sukhoverkhov, A. Tressaud, C. Labrugere, E. Durand, N.S. Chilingarov, L.N. Sidorov, J. Fluorine Chem. 127 (2006) 832–836.
[6] C. Cardinaud, A. Tressaud, in: T. Nakajima, B. Zemva, A. Tressaud (Eds.), Advanced Inorganic Fluorides, Elsevier, 2000, p. 437 (Chapter 14).
[7] A. Tressaud, E. Durand, C. Labrugère, A.P. Kharitonov, L.N. Kharitonova, J. Fluorine Chem. 128 (2007) 378–391.
[8] A. Tressaud, C. Labrugère, E. Durand, C. Brigouleix, R. Andriessen, Science China, Ser. E: Technol. Sci. 52 (2009) 104–110.
[9] E. Lataste, A. Demourgues, H. Leclerc, J.-M. Goupil, A. Vimont, E. Durand, C. Labrugère, H. Benalla, A. Tressaud, J. Phys. Chem. C 112 (2008) 10943–10951.
[10] A. Tressaud, C. Labrugère, E. Durand, H. Serier, L.P. Demyanova, J. Vac. Sci. Technol. A 28 (2010) 373–381.
[11] M.V. Gorev, I.N. Flerov, A. Tressaud, E. Durand, J. Phys.: Condens. Matter 14 (2002) 6447.
[12] F.J. Zúñiga, A. Tressaud, J. Darriet, J. Solid State Chem. 179 (2006) 3607–3614.
[13] I. Hernández, F. Rodríguez, A. Tressaud, Inorg. Chem. 47 (2008) 10288–10298.
[14] A. Tressaud, N. Bartlett, J. Solid State Chem. 162 (2001) 333.
[15] D. Pauwels, A. Demourgues, H. Laronze, P. Gravereau, F. Guillen, O. Isnard, A. Tressaud, Solid State Sci. 4 (2002) 1471.
[16] F. Goubin, X. Rocquefelte, D. Pauwels, A. Tressaud, A. Demourgues, S. Jobic, Y. Montardi, J. Solid State Chem. 177 (2004) 2833–2840.
[17] D. Pauwels, F. Weill, A. Tressaud, A. Demourgues, Chem. Mater. 18 (2006) 6121–6131.
[18] C. Legein, F. Fayon, C. Martineau, M. Body, J.-Y. Buzaré, D. Massiot, E. Durand, A. Tressaud, A. Demourgues, O. Péron, B. Boulard, Inorg. Chem. 45 (2006) 10636–10641.
[19] L. Sronek, J. Majimel, Y. Kihn, Y. Montardi, A. Tressaud, M. Feist, C. Legein, J.Y. Buzare, M. Body, A. Demourgues, Chem. Mater. 19 (21) (2007) 5110–5121.
[20] A. Demourgues, L. Francke, E. Durand, A. Tressaud, J. Fluorine Chem. 114 (2002) 229.
[21] L. Francke, E. Durand, A. Demourgues, A. Vimont, M. Daturi, A. Tressaud, J. Mater. Chem. 13 (2003) 2330.
[22] X. Rocquefelte, F. Goubin, Y. Montardi, N. Viadere, A. Demourgues, A. Tressaud, M.H. Whangbo, S. Jobic, Inorg. Chem. 44 (2005) 3589–3593.
[23] D. Dambournet, A. Demourgues, C. Martineau, S. Pechev, J. Lhoste, J. Majimel, A. Vimont, J.C. Lavalley, C. Legein, J.Y. Buzaré, F. Fayon, A. Tressaud, Chem. Mater. 20 (2008) 1459–1469.
[24] A. Demourgues, N. Penin, E. Durand, F. Weill, D. Dambournet, N. Viadere, Tressaud, Chem. Mater. 21 (7) (2009) 1275–1283.
[25] S. Rüdiger, U. Groß, E. Kemnitz, J. Fluorine Chem. 128 (2007) 353–368.
[26] E. Kemnitz, U. Groß, St. Rüdiger, S.C. Shekar, Angew. Chem. Int. Ed. 42 (2003) 4251–4254.
[27] S. Rüdiger, E. Kemnitz, Dalton Trans. (9) (2008) 1117–1127.
[28] S. Rüdiger, G. Eltanany, U. Groß, E. Kemnitz, J. Sol-Gel Sci. Technol. 41 (2007) 299–311.
[29] J.K. Murthy, U. Groß, St. Rüdiger, E. Kemnitz, J.M. Winfield, J. Solid State Chem. 179 (2006) 739–746.
[30] D. Dambournet, A. Demourgues, C. Martineau, E. Durand, J. Majimel, A. Vimont, H. Leclerc, J.C. Lavalley, M. Daturi, C. Legein, J.Y. Buzaré, F. Fayon, A. Tressaud, J. Mater. Chem. 18 (2008) 2483–2492.
[31] D. Dambournet, G. Eltanamy, A. Vimont, J.C. Lavalley, J.M. Goupil, A. Demourgues, E. Durand, J. Majimel, S. Rudiger, E. Kemnitz, J.M. Winfield, A. Tressaud, Chem. Eur. J. 14 (2008) 6205–6212.
[32] D. Dambournet, A. Demourgues, C. Martineau, J. Majimel, M. Feist, C. Legein, J.Y. Buzaré, F. Fayon, A. Tressaud, J. Phys. Chem. C 112 (2008) 12374–12380.
[33] D. Dambournet, A. Demourgues, C. Martineau, E. Durand, J. Majimel, C. Legein, J.Y. Buzare, F. Fayon, A. Vimont, H. Leclerc, A. Tressaud, Chem. Mater. 20 (22) (2008) 7095–7106.
[34] E. Kemnitz, St. Rüdiger, in: A. Tressaud (Ed.), Functionalized Inorganic Fluorides: Synthesis, Characterization and Properties of Nanostructured Solid, Wiley, 2010, pp. 69–100.
[35] J. Grannec, L. Lozano, in: P. Hagenmuller (Ed.), Inorganic Solid Fluorides, Academic Press, 1985, pp. 17–76.
[36] P. Daniel, A. Bulou, M. Rousseau, J. Nouet, J.L. Fourquet, M. Leblanc, R.J. Burriel, J. Phys.: Condens. Matter (1990) 5663.
[37] J.L. Fourquet, M. Rivière, A. Le Bail, Eur. J. Solid State Chem. 25 (1988) 535.
[38] A. Le Bail, C. Jacoboni, M. Leblanc, R. De Pape, H. Duroy, J.L. Fourquet, J. Solid State Chem. 77 (1988) 96.
[39] N. Herron, D.L. Thorn, R.L. Harlow, G.A. Jones, J.B. Parise, J.A. Fernandez-Baca, T. Vogt, Chem. Mater. 7 (1995) 75.
[40] S. Fujihara, M. Tada, T. Kimura, Thin Solid Films 304 (1997) 252–255.
[41] S. Fujihara, in: A. Tressaud (Ed.), Functionalized Inorganic Fluorides: Synthesis, Characterization and Properties of Nanostructured Solids, Wiley, 2010, pp. 307–330.
[42] N. Penin, N. Viadere, D. Dambournet, A. Tressaud, A. Demourgues, Mater. Res. Soc. Symp. Proc. (2006) 891.